Measurement of transient out-of-plane displacement gradients in plates using double-pulsed subtraction TV shearography

Antonio Fernández, MEMBER SPIE

Universidad de Vigo

Department of Engineering Design

Escuela Técnica Superior de Ingenieros Industriales

Campus Universitario Lagoas-Marcosende

E-36200 Vigo

Spain

Phone: +34 986 812 191

Fax: + 34 986 812 201

E-mail: antfdez@uvigo.es

Ángel F. Doval

Universidad de Vigo

Department of Applied Physics

Escuela Técnica Superior de Ingenieros Industriales

Campus Universitario Lagoas-Marcosende

E-36200 Vigo

Spain

Phone: +34 986 812 216

Fax: + 34 986 812 201

E-mail: adoval@uvigo.es

Guillermo H. Kaufmann, MEMBER SPIE

Consejo Nacional de Investigaciones Científicas y Técnicas y Universidad Nacional de Rosario

Instituto de Física de Rosario

Bv. 27 de Febrero 210 bis

2000 Rosario

Argentina

Tel. +54 (0)341 485-3200, 485-3222, Ext. 20

Fax +54 (0)341 482-1772

E-mail: guille@ifir.ifir.edu.ar

Abundio Dávila

Centro de Investigaciones en Óptica

Apartado Postal 1-948

37000 León-Gto

Mexico

Tel: + 52 47 731017-18

Fax: + 52 47 175000

E-mail: adavila@foton.cio.mx

Jesús Blanco-García

Universidad de Vigo

Department of Applied Physics

Escuela Unversitaria de Ingeniería Técnica Industrial

Torrecedeira 86

E-36208 Vigo

Spain

Phone: +34 986 813 681

Fax: + 34 986 813 663

E-mail: jblanco@uvigo.es

Carlos Pérez-López

Centro de Investigaciones en Óptica

Apartado Postal 1-948

37000 León-Gto

Mexico

Tel: + 52 47 731017-18

Fax: + 52 47 175000

E-mail: cperezl@foton.cio.mx

José L. Fernández

Universidad de Vigo

Department of Applied Physics

Escuela Técnica Superior de Ingenieros Industriales

Campus Universitario Lagoas-Marcosende

E-36200 Vigo

Spain

Phone: +34 986 812 216

Fax: + 34 986 812 201

E-mail: jlfdez@uvigo.es

Abstract. We report a technique for the measurement of transient out-of-plane displacement gradients in plane objects by double-pulsed subtraction TV shearography. The fringe patterns are automatically and quantitatively analyzed by the Fourier transform method. A novel optical setup based on the separation and further recombination of illumination beams is demonstrated for the generation of carrier fringes. The principle of the proposed technique is theoretically described and its immunity to environmental disturbances is discussed. Experimental results obtained with a metallic plate excited by the impact of a piezoelectric transducer are presented.

Subject terms: metrology; speckle interferometry; shearography; shock.

1 Introduction

TV shearography (TVS), or electronic speckle pattern shearing interferometry (ESPSI) as it is also known, is a nondestructive, whole-field technique that allows the measurement of spatial derivatives of displacements. Early research on shearing techniques used moiré fringes resulting of the superposition of two fringe patterns obtained by holographic interferometry.[1] Photographic film was later replaced by electronic devices, which avoid the somewhat expensive and time-consuming development process.[2] Gradient of displacement can also be obtained by the closely related TV holography (TVH) through image processing.[3] However, in applications that involve the measurement of spatial derivatives of displacement, e.g. strain analysis and detection of local defects in various materials, TVS outstrips TVH in several aspects. First, the calculation of spatial derivatives is a time-consuming operation, while TVS yields the slope of displacement directly. Second, due to its quasi-common path design, TVS is less sensitive than TVH to the influence of environmental disturbances, e.g., air turbulence, external vibration, rigid body motion, etc. Moreover, the requirement of a light source with large coherence length may be relaxed. And third, the possibility to change the sensitivity of the interferometer by adjusting the amount of shear broadens the measurement range of TVS.

The use of pulsed lasers in TVS relaxes even more the stability requirements for the experimental setup and makes possible the analysis of high-speed transient events. Nevertheless, only a few papers reporting on pulsed TVS have appeared. Spooren *et al.*[4] originally demonstrated the application of a double-pulsed laser to electronic speckle shear interferometry. Shear is introduced in the speckle interferograms by slightly tilting one of the mirrors in a Michelson type of shear interferometer,[5] and correlation fringe

patterns are formed by double-pulse subtraction,[6] a technique formerly proposed for TVH. Emphasis was given to the study of fringe visibility rather than to the implementation of a phase evaluation method, and hence measurements remain qualitative. The first quantitative measurements of spatial derivatives of displacement using double-pulsed TVS have been carried out by Pedrini *et al.*[7] They use a Mach-Zehnder interferometer after the imaging lens in order to record the interference between two sheared images on a CCD. Lateral shear between these two images is adjusted by shifting one mirror in the setup and spatial carrier is introduced in the speckle shear interferograms by tilting one mirror (or one beam splitter). Interference phase is evaluated using either the Fourier transform[8] or the spatial-carrier phase-shifting[9] methods. The optical phase change due to object's deformation is obtained as the difference between phase distributions calculated from two different speckle shear interferograms recorded before and after deformation, respectively. More recently, Dávila *et al.*[10] have applied pulsed TVS to quantitatively measure the slope of transient displacements following a different approach. Spatial carrier is introduced in the correlation fringe patterns rather than in the speckle shear interferograms by translating manually the diverging lens that expands the illumination beam along its optical axis. Phase is then evaluated by the spatial synchronous detection method.[11] The technique has been experimentally demonstrated in laboratory conditions. Unfortunately, the long time required for the lens translation (several seconds) negates the advantages of pulsed TVS and prevents its application in industrial environments. Bonding the diverging lens to a piezoelectric translator significantly improves the immunity of the system to environmental disturbances. This solution has been adopted in a double-pulsed addition TVH system for harmonic vibration measurement.[12] However, it has been found that the use of a piezo-mounted lens to generate carrier

fringes still imposes a lower limit to the minimum separation between laser pulses because of the response time of the piezoelectric element.

In this paper, we report a novel technique for the measurement of transient out-of-plane displacement gradients using double-pulsed subtraction TVS and the Fourier transform method (FTM). We have developed a new optical setup without moving devices to introduce spatial carrier in the fringe patterns by changing the sensitivity vector between laser pulses. In contrast to the technique described in Ref. 10, the only lower limit to the minimum time separation between laser pulses is imposed by the charge transfer period of the CCD, which can be as low as ~ 100 ns in the latest models of the so called double-flash CCD cameras.[13]

2 Principle of the technique

In this section we firstly present the general expression of a double-pulsed subtraction TVS fringe pattern. Later, we derive the phase difference increment due to combined mechanical excitation and the proposed technique for spatial carrier generation. Finally, we calculate the gradient of out-of-plane displacement by the FTM. Throughout this section we use certain approximations that allow phase difference increment calculations to be reduced to more simple mathematical manipulations.

A. Fringe formation in double-pulsed subtraction TVS

In double-pulsed subtraction TVS the CCD camera records two speckle shear interferograms in separated video fields.[6] The first laser pulse is fired with the object at rest, and the corresponding intensity distribution may be expressed as

$$I_1(\mathbf{x}) = I_{\mathrm{m}}(\mathbf{x})[1 + V(\mathbf{x})\cos\Delta\psi_1(\mathbf{x})], \tag{1}$$

where $I_{\mathrm{m}}(\mathbf{x})$ and $V(\mathbf{x})$ are the mean intensity and the visibility of the speckle shear interferogram at a point $\mathbf{x}=(x,y,L)$ of the object's surface, respectively. It should be

emphasized that only plane objects are considered in this paper. Some time later (typically tens of microseconds) the object is stressed and the laser emits a second pulse properly timed with respect to the mechanical excitation. The resulting intensity distribution is given by

$$I_2(\mathbf{x}) = I_{\mathrm{m}}(\mathbf{x})[1 + V(\mathbf{x})\cos\Delta\psi_2(\mathbf{x})], \tag{2}$$

being the terms $\Delta\psi_1(\mathbf{x})$ and $\Delta\psi_2(\mathbf{x})$ the difference between the phases of the interfering speckle patterns for the first and the second speckle shear interferograms, respectively.

Subtraction of intensity distributions (1) and (2) once they have been digitized, and subsequent full wave rectification, yields a speckled, high visibility correlation fringe pattern

$$I(\mathbf{x}) = |gI_2(\mathbf{x}) - gI_1(\mathbf{x})| = 2gI_{\mathrm{m}}(\mathbf{x})V(\mathbf{x})\left|\sin\frac{\Delta\psi_1(\mathbf{x}) + \Delta\psi_2(\mathbf{x})}{2}\right|\left|\sin\frac{\Delta\phi(\mathbf{x})}{2}\right|, \tag{3}$$

where $g = g(\lambda)$ is the spectral sensitivity of the camera for the laser wavelength λ and $\Delta\phi(\mathbf{x})$ is the phase difference increment

$$\Delta\phi(\mathbf{x}) = \Delta\psi_2(\mathbf{x}) - \Delta\psi_1(\mathbf{x}). \tag{4}$$

It should be noted that the modulus operation in Eq. (3) introduces harmonic distortion in the fringe pattern, which can give rise to significant errors in the recovered phase. This is why we use quadratic detection rather than full wave rectification for fringe analysis purposes

$$i(\mathbf{x}) = I^2(\mathbf{x}) = i_{\mathrm{m}}(\mathbf{x})[1 - \cos\Delta\phi(\mathbf{x})], \tag{5}$$

where the local mean intensity of the fringe pattern is given by

$$i_{\mathrm{m}}(\mathbf{x}) = 2g^2 I_{\mathrm{m}}^2(\mathbf{x})V^2(\mathbf{x})\sin^2\frac{\Delta\psi_1(\mathbf{x}) + \Delta\psi_2(\mathbf{x})}{2}. \tag{6}$$

B. Phase difference in double-pulsed subtraction TVS

According to the geometry depicted in Fig. 1, the optical phase of one of the interfering speckle patterns produced by the first laser pulse may be expressed as

$$\psi_1(\mathbf{x}) = \psi_i + \psi_{F1} + \frac{2\pi}{\lambda} R_1(\mathbf{x}) + \psi_s(\mathbf{x}) + \psi_{P1}(\mathbf{x}), \tag{7}$$

with ψ_i the initial phase of the light source, ψ_{F1} and $\psi_{P1}(\mathbf{x})$ the phase changes due to the propagation of light from the laser to the focus F_1 and from a point P_1 on the object surface to the image plane, respectively, $\psi_s(\mathbf{x})$ a random phase term due to the object surface roughness, and $R_1(\mathbf{x})$ the distance from the focus F_1 to the point P_1 on the object.

In TVS, a point in the image plane receives contributions from two or more points on the object.[14] Let us consider a situation when the points on the object $\mathbf{x}$ and $\mathbf{x}+\delta\mathbf{x}$ are imaged at the same point on the image plane, being $\delta\mathbf{x} = (\delta x, \delta y)$ the object plane shear. In that case, the phase difference of the first speckle shear interferogram is given by

$$\Delta\psi_1(\mathbf{x}) = \frac{2\pi}{\lambda}[R_1(\mathbf{x}+\delta\mathbf{x}) - R_1(\mathbf{x})] + \psi_s(\mathbf{x}+\delta\mathbf{x}) - \psi_s(\mathbf{x}) + \psi_{P1}(\mathbf{x}+\delta\mathbf{x}) - \psi_{P1}(\mathbf{x}). \tag{8}$$

Making a first order approximation

$$R_1(\mathbf{x}+\delta\mathbf{x}) - R_1(\mathbf{x}) \approx \frac{\partial R_1(\mathbf{x})}{\partial x}\delta x + \frac{\partial R_1(\mathbf{x})}{\partial y}\delta y = \nabla R_1(\mathbf{x})\delta\mathbf{x}, \tag{9}$$

Eq. (8) may be rewritten as follows

$$\Delta\psi_1(\mathbf{x}) = \frac{2\pi}{\lambda}\nabla R_1(\mathbf{x})\delta\mathbf{x} + \psi_s(\mathbf{x}+\delta\mathbf{x}) - \psi_s(\mathbf{x}) + \nabla\psi_{P1}(\mathbf{x})\delta\mathbf{x}. \tag{10}$$

C. Spatial carrier generation

The object surface undergoes a local displacement $\mathbf{u}(\mathbf{x}) = [u(\mathbf{x}), v(\mathbf{x}), w(\mathbf{x})]$ because of mechanical excitation between exposures. Let us now suppose that the first and the

second laser pulses propagate through separated paths, as shown in Fig. 1. Assuming that neither the object displacement nor the change in the illumination geometry introduce speckle decorrelation, the optical phase of the speckle pattern corresponding to the second laser pulse may then be expressed as

$$\psi_2(\mathbf{x}) = \psi_i + \psi_{F2} + \frac{2\pi}{\lambda} R_2(\mathbf{x}) + \psi_s(\mathbf{x}) + \psi_{P2}(\mathbf{x}). \tag{11}$$

where $\psi_{F2}(\mathbf{x})$ and $\psi_{P2}(\mathbf{x})$ are the phase changes due to the propagation of light from the laser to the focus F_2 and from a point P_2 on the displaced object surface to the image plane, respectively, and $R_2(\mathbf{x})$ is the distance from the focus F_2 to the point P_2 on the object.

In a first order approximation, the phase difference of the second speckle shear interferogram is given by

$$\Delta\psi_2(\mathbf{x}) = \frac{2\pi}{\lambda} \nabla R_2(\mathbf{x}) \delta\mathbf{x} + \psi_s(\mathbf{x} + \delta\mathbf{x}) - \psi_s(\mathbf{x}) + \nabla\psi_{P2}(\mathbf{x}) \delta\mathbf{x}. \tag{12}$$

Provided that the in-plane components of the object displacement are negligible and that the object surface is placed perpendicular to the observation direction, we can approximate the difference of the phase changes due to the propagation of light from the points P_1 and P_2 to the image plane by

$$\psi_{P2}(\mathbf{x}) - \psi_{P1}(\mathbf{x}) \approx \frac{2\pi}{\lambda} w(\mathbf{x}), \tag{13}$$

and hence

$$[\nabla\psi_{P2}(\mathbf{x}) - \nabla\psi_{P1}(\mathbf{x})]\delta\mathbf{x} \approx \frac{2\pi}{\lambda} \nabla w(\mathbf{x}) \delta\mathbf{x}. \tag{14}$$

Thus, Eq. (4) may be rewritten in the form

$$\Delta\phi(\mathbf{x}) = \frac{2\pi}{\lambda} \nabla[R_2(\mathbf{x}) - R_1(\mathbf{x}) + w(\mathbf{x})]\, \delta\mathbf{x}\,. \tag{15}$$

Referring to Fig. 1, we can write

$$R_1(\mathbf{x}) = \left(x^2 + y^2 + L^2\right)^{1/2}, \tag{16}$$

$$R_2(\mathbf{x}) = \left\{x^2 + y^2 + \left[L + w(\mathbf{x}) - d\right]^2\right\}^{1/2}, \tag{17}$$

and introducing Eqs. (16) and (17) in Eq. (15) yields the rather long result

$$\Delta\phi(\mathbf{x}) = \frac{2\pi}{\lambda}\left(\left\{\frac{x + \left[L + w(\mathbf{x}) - d\right]\dfrac{\partial w(\mathbf{x})}{\partial x}}{\sqrt{x^2 + y^2 + \left[L + w(\mathbf{x}) - d\right]^2}} - \frac{x}{\sqrt{x^2 + y^2 + L^2}} + \frac{\partial w(\mathbf{x})}{\partial x}\right\}\delta x \right.$$
$$\left. + \left\{\frac{y + \left[L + w(\mathbf{x}) - d\right]\dfrac{\partial w(\mathbf{x})}{\partial y}}{\sqrt{x^2 + y^2 + \left[L + w(\mathbf{x}) - d\right]^2}} - \frac{y}{\sqrt{x^2 + y^2 + L^2}} + \frac{\partial w(\mathbf{x})}{\partial y}\right\}\delta y\right). \tag{18}$$

Obviously, direct application of this general equation involves a huge mathematical complexity. However, if we introduce certain approximations, calculations are reduced to simple linear operations. Our approximations will be based on two assumptions: (a) the distance L between the focus F_1 and the object plane is much greater than any other distance which appear in Eq. (18) and (b) the distance d between the foci F_1 and F_2 is much greater than the out-of-plane displacement $w(\mathbf{x})$. These assumptions may be formalized as follows

$$L >> x \quad , \quad L >> y\,, \tag{19a}$$

$$L >> d >> w(\mathbf{x}). \tag{19b}$$

If the conditions above are satisfied, we can make a further approximation

$$\frac{ax + by}{\sqrt{x^2 + y^2 + L^2}} \approx \frac{a}{L}x + \frac{b}{L}y\,, \tag{20}$$

where a and b are coefficients.

Taking into account Eqs. (19) and (20) allows Eq. (18) to be rewritten as

$$\Delta\phi(\mathbf{x}) = 2\pi\frac{d\delta x}{\lambda L^2}x + \frac{4\pi\delta x}{\lambda}\frac{\partial w(\mathbf{x})}{\partial x} + 2\pi\frac{d\delta y}{\lambda L^2}y + \frac{4\pi\delta y}{\lambda}\frac{\partial w(\mathbf{x})}{\partial y}. \tag{21}$$

This result demonstrates that the phase difference increment in double-pulsed subtraction TVS with separated optical paths is the sum of two terms proportional to the spatial derivatives of displacement across horizontal and vertical coordinates as well as two terms proportional to the coordinates themselves. These last two terms may be considered as a spatial carrier whose frequency components (in units of fringes per image) are

$$f_{cx} = \frac{d\delta x X}{\lambda L^2}, \tag{22}$$

$$f_{cy} = \frac{d\delta y Y}{\lambda L^2}, \tag{23}$$

where X and Y are the horizontal and vertical fields of view, respectively.

D. Quantitative determination of the out-of-plane displacement gradient

The phase difference increment (21) can be extracted from the fringe pattern (5) by the FTM[8]

$$\Delta\phi(\mathbf{x}) = \mathrm{unw}\left\{\tan^{-1}\left\{\frac{\mathrm{Im}[\Im^{-1}\{\Im\{i(\mathbf{x})\}W(\mathbf{f})\}]}{\mathrm{Re}[\Im^{-1}\{\Im\{i(\mathbf{x})\}W(\mathbf{f})\}]}\right\}\right\}, \tag{24}$$

where $\Im$ is the 2-D Fourier transform, $W(\mathbf{f})$ is a suitable window in the Fourier plane, and unw denotes a generic phase-unwrapping operation.

Finally, to calculate the out-of-plane displacement gradient we proceed as follows. First, we introduce pure horizontal shear (δy=0) together with optical path

separation. The resulting fringe pattern shows a set of vertical, equally spaced carrier fringes modulated by the transient deformation. We denote the corresponding phase difference increment by $\Delta\phi_x^{\mathrm{d}}(\mathbf{x})$. In order to isolate the term proportional to the displacement derivative we subtract the carrier contribution from the recovered phase. This method is called subtraction of the phase of the undeformed carrier fringes (SPUCF).[15] The carrier contribution in the horizontal direction $\Delta\phi_x^{\mathrm{c}}(\mathbf{x})$ is evaluated from a fringe pattern obtained without mechanical excitation. Next, the interferometer is arranged to introduce pure vertical shear (δx=0) so that the resulting carrier fringes are now a set of horizontal, equally spaced fringes. The experiment is then repeated with and without mechanical excitation. We denote the corresponding phase difference increments by $\Delta\phi_y^{\mathrm{d}}(\mathbf{x})$ and $\Delta\phi_y^{\mathrm{c}}(\mathbf{x})$, respectively. Gradient determination is straightforward from these definitions

$$\nabla w(\mathbf{x}) = \frac{\lambda}{4\pi}\left(\frac{\Delta\phi_x^{\mathrm{d}}(\mathbf{x}) - \Delta\phi_x^{\mathrm{c}}(\mathbf{x})}{\delta x}, \frac{\Delta\phi_y^{\mathrm{d}}(\mathbf{x}) - \Delta\phi_y^{\mathrm{c}}(\mathbf{x})}{\delta y}\right). \tag{25}$$

3 Optical setup

Our experimental setup for spatial carrier generation in double-pulsed TVS is shown in Fig. 2. The light source consists of two separate *Q*-switched Nd:YAG oscillators, commonly seeded by a diode-pumped Nd:YAG *cw* laser to obtain mutual coherence between their beams. The infrared outputs are combined at BC1 before passing through a frequency-doubling crystal that makes alignment tasks and signal detection safer and easier. Moreover, the sensitivity of the interferometer is multiplied by a factor of two. Each cavity produces 12 mJ in 20-ns pulses at λ = 532 nm at a rate of 25 Hz. Giving a small tilt to mirror M4, the green radiation produced by cavity 1 goes through a different path than light produced by cavity 2. Both beams are expanded through

diverging lenses and then are made collinear at BC2. The lens NL2 is placed a distance d (exaggerated in the diagram for clarity) nearer to BC2 than NL1, and therefore the curvature radius of the illumination beam is greater for the first laser pulse than for the second, as required for spatial carrier generation (Fig. 1). The lens NL2 is mounted on a translation stage that allows the distance d to be precisely adjusted. Either horizontal or vertical shear is introduced in the speckle interferograms by slightly tilting the mirror M9 in the Michelson arrangement placed in front of the imaging system.

4 Experimental results

We have demonstrated the optical setup schematically represented in Fig. 2 for the measurement of the out-of-plane displacement gradient of impact-induced transient bending waves in metallic plates. The operation of our double-pulsed TVS system is as follows. The laser continuously emits twin-pulses at a rate of 25 Hz, properly timed with respect to the video signal. When the operator gives the order to start, the test object receives an impact from a piezoelectric transducer, and a video frame is digitized and stored as 512×512×8 bits in a frame grabber. The irradiance values recorded by the CCD during both the first and the second laser pulses, Eqs. (1) and (2), are contained in the even and the odd lines of that image, respectively. Intensity fluctuations between first and second laser pulses are digitally compensated. Next, a frame processor subtracts even lines from the adjacent odd ones and rectifies the result, Eq. (3), yielding a set of equally-spaced straight carrier fringes modulated by the spatial derivative of normal displacement. (The interested reader is addressed to references 16 and 17 for further details on the synchronism system).

The specimen used in our experiment is an aluminum plate (300 mm × 120 mm × 3.5 mm) clamped along its left and its right edges. An area of approximately 124 mm (X) × 84 mm (Y) was measured. The object was impact-excited at the central point of

the back side of this area. Time separation between laser pulses was set to 50 μs. Delay between the piezoelectric transducer driving signal and the firing of the second laser pulse was adjusted to 20 μs by means of a programmable delay generator. We set the distances d and L to 6.35 mm and 2.09 m, respectively. The numerical values of horizontal and vertical object shear are $\delta x = 32.5$ mm and $\delta y = 37$ mm, respectively. One can calculate horizontal as well as vertical carrier frequencies using Eqs. (22) and (23). For the experimental conditions just mentioned, the theoretical values are $f_{cx} = 11.01$ and $f_{cy} = 8.49$, expressed in fringes per image. These predictions are in good agreement with experimental results.

Fig. 3(a) is an experimental fringe pattern obtained with pure horizontal shear, which shows vertical carrier fringes modulated by the transient deformation. Fig. 3(b) is the fringe pattern resulting of the repetition of the experiment without mechanical excitation. Application of the FTM, Eq. (24), to the fringe patterns in Figs. 3(a) and 3(b) yields $\Delta\phi_x^{\mathrm{d}}(\mathbf{x})$ and $\Delta\phi_x^{\mathrm{c}}(\mathbf{x})$, respectively (see section 2.D). We used a filtering window $W(\mathbf{f})$ that yields one for the points inside a circle and 0 otherwise. Following the approach of Takatsuji *et al.*,[18] we set the frequency coordinates of the center of this circular domain to the same values as the peak of the sidelobe of the Fourier spectrum and its diameter to the maximum value that yields a phase map without strong discontinuities (15 pixels for the fringe patterns in Fig. 3). Wrapped phase maps were unwrapped using an algorithm based on a least-squares minimization technique that is solvable by the discrete cosine transform.[19] In this approach, invalid pixels due to phase inconsistencies and regions with missing data are excluded from the unwrapping process through the assignment of zero-valued weights. In this way, the algorithm can smoothly interpolate the phase over pixels with bad data. The weighted problem is solved using a preconditioned conjugate-gradient method, which gives guaranteed and

faster convergence. The spatial derivative along the horizontal direction can be determined by subtracting $\Delta\phi_x^{\mathrm{d}}(\mathbf{x})$ from $\Delta\phi_x^{\mathrm{c}}(\mathbf{x})$ and scaling the result, Fig. 3(c). Following an analogous procedure, we evaluated the phase distributions $\Delta\phi_y^{\mathrm{d}}(\mathbf{x})$ and $\Delta\phi_y^{\mathrm{c}}(\mathbf{x})$ from their corresponding experimental fringe patterns obtained with pure vertical shear, Figs. 3(d) and 3(e), to determine the spatial derivative along the vertical direction, Fig. 3(f). Finally, Fig. 4 is a representation of the out-of-plane displacement gradient.

5 Discussion

We have developed an optical setup for spatial carrier generation without moving parts. This makes our system highly immune to environmental disturbances because time separation between laser pulses can be as short as the transfer period of the CCD camera (see Section 1). However, the inherent immunity to noise of our system is strongly affected by the method employed for carrier removal. We have used SPUCF because it is the carrier removal method that introduces lower errors in the phase distribution, nevertheless the immunity to environmental disturbances is dramatically reduced due to the relatively long time elapsed between the recording of the two necessary fringe patterns (40 ms). This fact may be disregarded as long as the working conditions are controlled, as it happens in a laboratory, although it is relevant for operation in industry. In this case, phase must be calculated from a single fringe pattern, and therefore SPUCF is inadequate. The solution is to use other carrier removal methods, e.g. translation of the sidelobe to the frequency origin or least-squares fit, which do not require a second fringe pattern for phase evaluation. The influence of the main existing carrier removal methods over the accuracy of the results as well as the immunity to noise is discussed in more depth in Ref. 15.

Obviously, the arguments above are completely true only for the calculation of one component of the displacement gradient, either the horizontal or the vertical spatial derivative, because of the long time required (tens of seconds) to repeat the experiment with a different shear direction.

Finally, it is possible to obtain a sequence of quantitative measurements showing the temporal evolution of the measured magnitude by repeating the experiment with a variable time delay between the mechanical impact and the second laser pulse.

6 Conclusions

We have reported a new technique for the measurement of transient out-of-plane displacement derivatives by double-pulsed subtraction TV shearography. The introduction of carrier fringes by mismatching the distances from the diverging lenses to the beam combiner allows quantitative analysis of the fringe patterns using the Fourier transform method. The inherent immunity to noise of our system, which is a valuable feature for industrial application, is strongly affected by the method employed for carrier removal. We have shown experimental results with a metallic plate excited by impact to illustrate the performance of our approach.

Acknowledgments

The authors thank for their support the following institutions: Xunta de Galicia (XUGA 32105B97), Comisión Interministerial de Ciencia y Tecnología (TAP97-0829-C03-01) and Universidad de Vigo (64502I801). Part of this work was presented at the SPIE's International Symposium on Optical Science, Engineering and Instrumentation.[20]

References

1. P. Boone and R. Verbiest, "Application of hologram interferometry to plate deformation and translation measurements", *Optica Acta* **16**, 555-567 (1969).

2. S. Nakadate, T. Yatagai, and H. Saito, "Digital speckle-pattern shearing interferometry", *Appl. Opt.* **19**, 4241-4246 (1980).

3. E. Vikhagen, "Nondestructive testing by use of TV holography and deformation phase gradient calculation", *Appl. Opt.* **29**, 137-144 (1990).

4. R. Spooren, A. A. Dyrseth, and M. Vaz, "Electronic shear interferometry: application of a (double-) pulsed laser", *Appl. Opt.* **32**, 4719-4727 (1993).

5. P. K. Rastogi, "Techniques of displacement and deformation measurements in speckle metrology", in *Speckle Metrology*, R. S. Sirohi, Ed., pp. 41-98, Marcel Dekker Inc., New York (1993).

6. R. Spooren, "Double-pulse subtraction TV holography", *Opt. Eng.* **31**, 1000-1007 (1992).

7. G. Pedrini, Y.-L. Zou, and H. J. Tiziani, "Quantitative evaluation of digital shearing interferogram using the spatial carrier method", *Pure Appl. Opt.* **5**, 313-321 (1996).

8. M. Takeda, H. Ina, and S. Kobayashi, "Fourier-transform method of fringe-pattern analysis for computer-based topography and interferometry", *J. Opt. Soc. Am.* **72**, 156-160 (1981).

9. M. Kujawinska, "Spatial phase measurement methods", in *Interferogram Analysis*, D. W. Robinson and G. T. Reid, Eds., pp. 141-193, Institute of Physics Press, Bristol (1993).

10. A. Dávila, G. H. Kaufmann, and C. Pérez-López, "Transient deformation analysis using a carrier method of pulsed electronic speckle-shearing pattern interferometry", *Appl. Opt.* **37**, 4116-4122 (1998).

11. K. H. Womack, "Interferometric phase measurement using spatial synchronous detection", *Opt. Eng.* **23**, 391-395 (1984).

12. A. J. Moore and C. Pérez-López, "Fringe carrier methods in double-pulsed addition ESPI", *Opt. Commun.* **141**, 203-212 (1997).

13. W. Steinchen, L. X. Yang, G. Kupfer, P. Mäckel, and F. Vössing, "Developmental steps to double pulse shearography" in *Laser Interferometry IX: Techniques and Analysis*, M. Kujawinska, G. M. Brown and M. Takeda, Eds., Proc. SPIE **3478**, 344-351 (1998).

14. R. S. Sirohi, "Speckle methods in experimental mechanics", in *Speckle Metrology*, R. S. Sirohi, Ed., pp. 99-156, Marcel Dekker Inc., New York (1993).

15. A. Fernández, G. H. Kaufmann, A. F. Doval, J. Blanco-García and J. L. Fernández, “Comparison of carrier removal methods in the analysis of TV holography fringes by the Fourier transform method”, *Opt. Eng.* **37**, 2899-2905 (1998).

16. A. Fernández, A. J. Moore, C. Pérez-López, A. F. Doval, and J. Blanco-García, "Study of transient deformations with pulsed TV holography: application to crack detection", *Appl. Opt.* **36**, 2058-2065 (1997).

17. A. Fernández, J. Blanco-García, A. F. Doval, J. Bugarín, B. V. Dorrío, C. López, J. M. Alén, M. Pérez-Amor, and J. L. Fernández, "Transient deformation measurement by double-pulsed-subtraction TV holography and the Fourier transform method", *Appl. Opt.* **37**, 3440-3446 (1998).

18. T. Takatsuji, B. F. Oreb, D. I. Farrant, and J. R. Tyrer, "Simultaneous measurement of three orthogonal components of displacement by electronic speckle-pattern interferometry and the Fourier transform method", *Appl. Opt.* **36,** 1438-1445 (1997).

19 G. H. Kaufmann, G. E. Galizzi and P. D. Ruiz, "Evaluation of a preconditioned conjugate-gradient algorithm for weighted least-squares unwrapping of digital speckle-pattern interferometry phase maps," *Appl. Opt.* **34,** 3076-3084 (1998).

20. A. Fernández, A. F. Doval, A. Dávila, J. Blanco-García, C. Pérez-López and J. L. Fernández, "Double-pulsed carrier speckle-shearing pattern interferometry for transient deformation analysis", in *Laser Interferometry IX: Techniques and Analysis*, M. Kujawinska, G. M. Brown and M. Takeda, Eds., Proc. SPIE **3478**, 352-358 (1998).

Figure captions

Fig. 1. Geometry of the optical path separation approach.

Fig. 2. Schematic experimental setup used to generate carrier fringes in double-pulsed-subtraction TV shearography: BS, beam splitter; BC1-BC3, beam combiners; M1-M9, mirrors; NL1 and NL2, negative lenses (their foci are shifted by a distance *d*).

Fig. 3. Transient bending waves in a metal plate 25 μs after mechanical excitation: (a)-(c) horizontal shear; (d)-(f) vertical shear; (b,e) carrier fringes; (a,d) corresponding double-pulsed-subtraction TV shearography fringe patterns, deformation plus carrier; (c,f) three-dimensional plots of the spatial derivatives of the out-of-plane displacement.

Fig. 4. 2-D representation of the transient out-of-plane displacement gradient in the central area of the tested specimen.

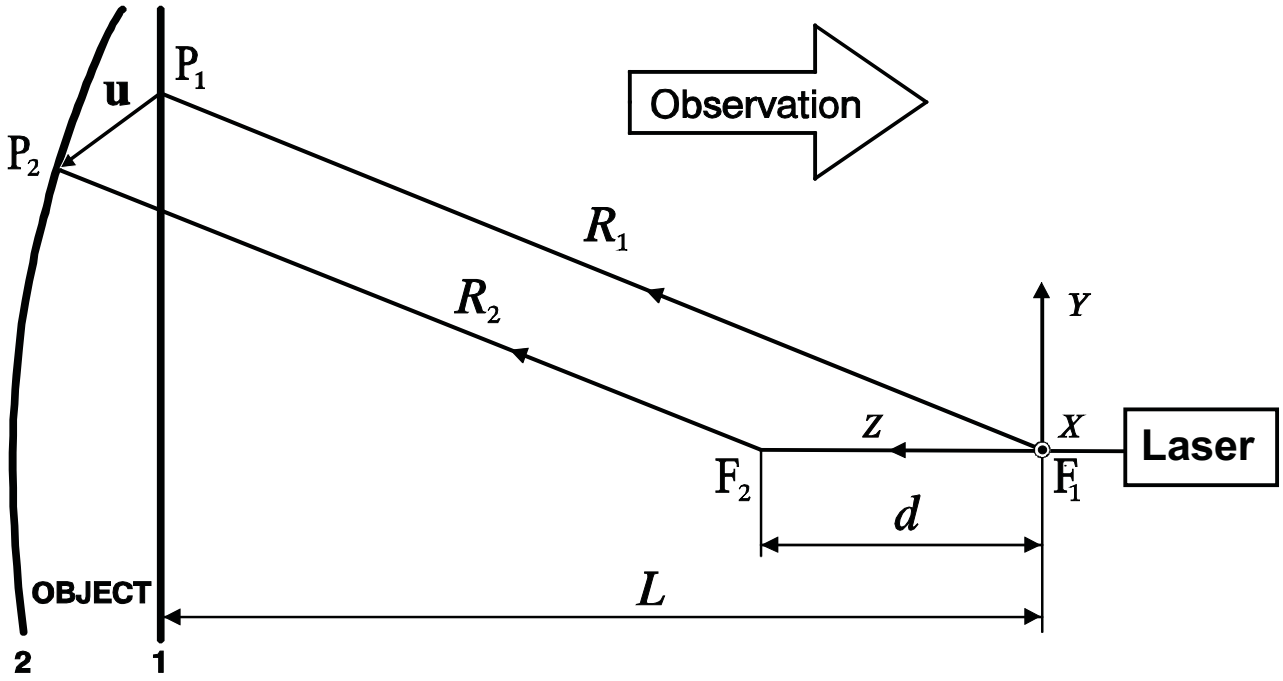

Figure 1
A. Fernández
Optical Engineering

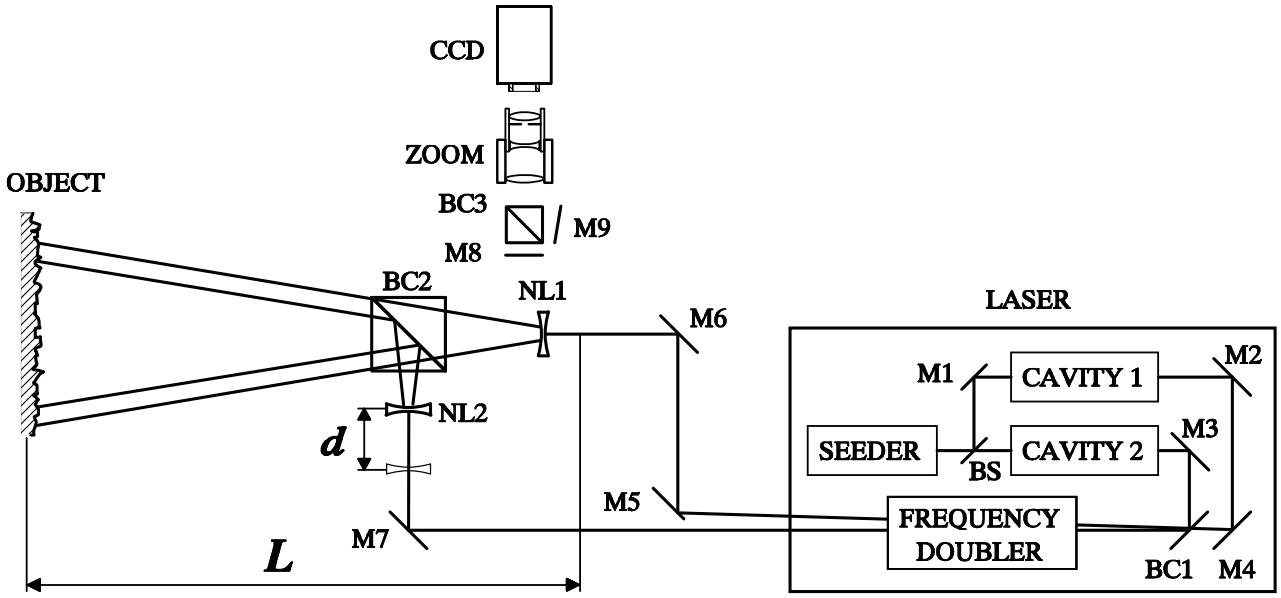

Figure 2
A. Fernández
Optical Engineering

(Note: Please, reduce to two-column width)

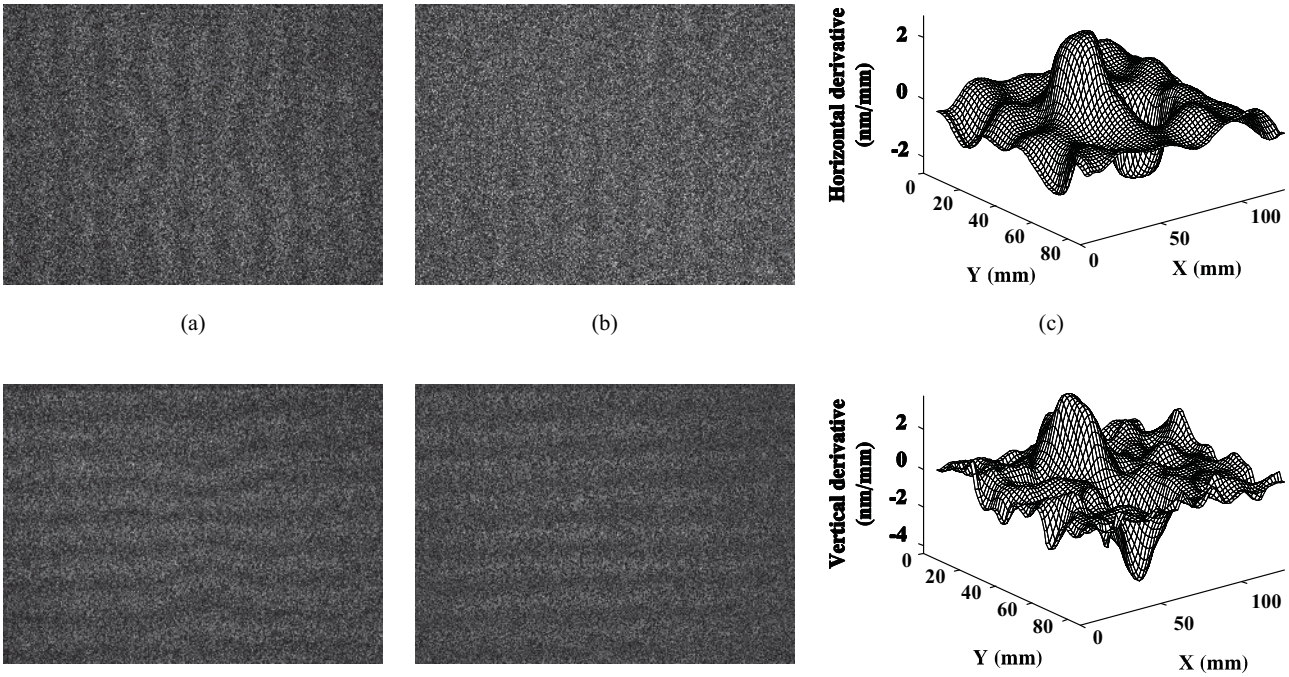

(a) (b) (c)

(d) (e) (f)

Figure 3
A. Fernández
Optical Engineering

(Note: Please, reduce to two-column width)

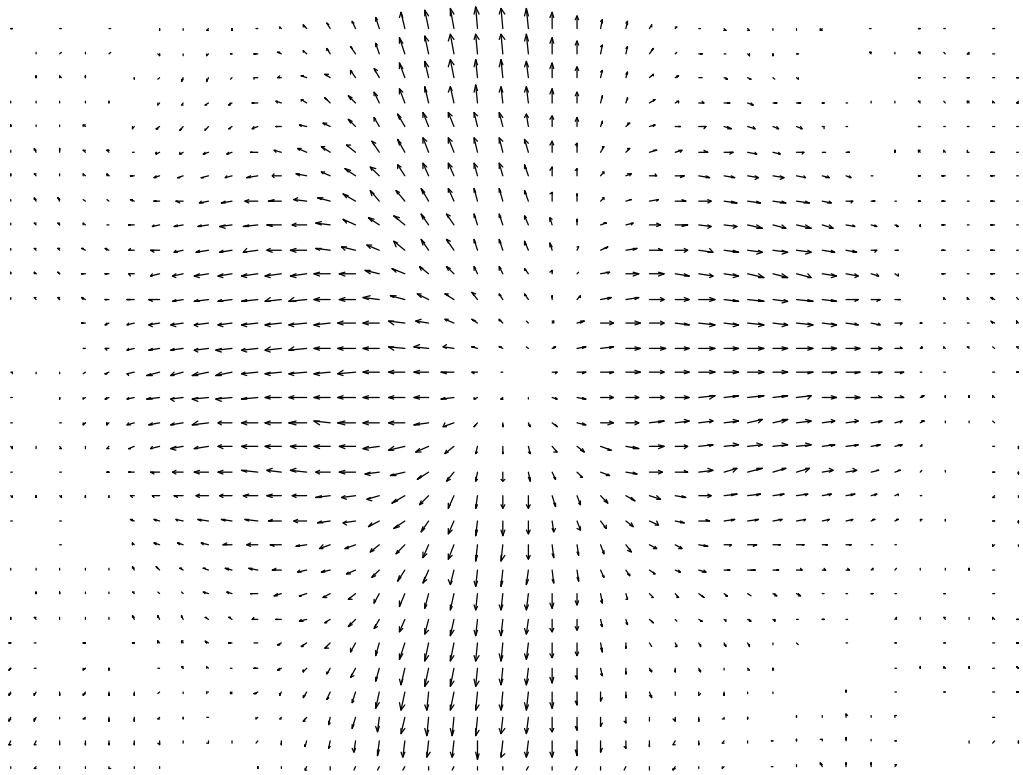

Figure 4
A. Fernández
Optical Engineering